

Highlights

Frequency domain laser ultrasound for inertial confinement fusion target wall thickness measurements

Martin Rzy, Guqi Yan, Clemens Grünsteidl, Georg Watzl, Kevin Sequoia, Pavel Lapa, Haibo Huang

- Resolved sub-micron thickness variations of mm-scale high-density carbon shells
- Spherical shell acoustic spectrum exhibits plate- and circumferential-resonances
- Dispersion relation contains Lamb-modes superimposed by circumferential resonances
- Zero-group-velocity plate resonances can be isolated for wall thickness determination
- Finite element wave propagation simulation in spherical shell

Frequency domain laser ultrasound for inertial confinement fusion target wall thickness measurements

Martin Rzy^a, Guqi Yan^{a,*}, Clemens Grünsteidl^b, Georg Watzl^b, Kevin Sequoia^b, Pavel Lapa^b and Haibo Huang^b

^aResearch Center for Non Destructive Testing, Science Park 2 / 2. OG, Altenberger Straße 69, Linz, 4040, Austria

^bGeneral Atomics, Energy Group, Inertial Fusion Technology Division, San Diego, 92121, CA, USA

ARTICLE INFO

Keywords:

frequency domain laser ultrasound
zero-group-velocity resonances
thickness measurement
inertial confinement fusion
spherical shell
circumferential resonances
finite element method

ABSTRACT

In inertial confinement fusion experiments hollow, spherical mm-sized capsules are used as a container for nuclear fuel. To achieve maximum implosion efficiency, a perfect capsule geometry is required. This paper presents a wall thickness measurement method based on zero-group velocity guided elastic wave resonances. They are measured with a non-destructive, contactless frequency domain laser ultrasound microscopy system. Wall thickness measurements along the equator of a high-density carbon capsule with a diameter of around 2 mm and a wall thickness of around 80 μm excellently agree with infrared interferometry reference measurements. In addition, the multi-resonant nature of a spherical shell is studied by complementing experimental observations with plate dispersion calculations and finite element wave propagation simulations. The presented method is scalable and can be applied to a broad range of target materials, including metals, or metal-doped targets.

1. Introduction

The implementation of nuclear fusion reactions under controlled laboratory conditions is one of the most challenging scientific and technological endeavors of our time. Yet it has the potential to significantly contribute to liberating us from the dependency on fossil fuel-based energy production. One of the most promising approaches in nuclear fusion research is inertial confinement fusion (ICF) [1]. Using that technique, a net target energy gain has been recently achieved in ignition experiments conducted at the National Ignition Facility (NIF) at the Lawrence Livermore National Laboratory in California, USA [2].

The deuterium-tritium fuel forms a uniform ice-layer on the interior of a mm-sized spherical ablator target capsule made of high-density carbon (HDC) or other materials [3, 4, 5, 6]. To reach the extreme temperature and pressure to start a fusion reaction, the capsule is compressed by repulsive forces created by abrupt target material ablation initiated by X-ray irradiation. As this mechanism sets high demands on target material quality and symmetry [6, 7, 8], precise, non-destructive characterization methods are required, which enable the selection of the most promising capsules for the high-yield ignition fusion experiments. One of the key parameters is the wall thickness uniformity of the capsules. HDC capsules have a thickness variation rejection criterion of 0.35 μm out of an average wall thickness of 80 μm . For optically transparent or translucent target materials, such as poly(α -methylstyrene), polystyrene and glow discharge polymer plastic capsules, the wall thickness can be determined by optical methods like infrared interferometry for

instance [9]. However, for any opaque target materials like metals, or metal-doped materials, optical methods are limited due to the low optical penetration depth. As an alternative, X-ray imaging can be used for this class of samples. Due to limited sensor array size and the need to fit the entire 2 mm capsule within the field of view, the ultimate wall thickness variation measurement precision is around $\pm 0.15 \mu\text{m}$, or more than one third of the wall thickness nonuniformity allowed for HDC capsules. Considering that future shells can be bigger and made of higher-Z metals, not every capsule is imageable by X-ray transmission imaging. Thus, to pave the way for a broader range of target materials, alternative wall thickness measurement techniques are required.

Ultrasonic elastic waves also penetrate optically absorbing or reflective solids, and thus are suitable for gauging their thickness [10, 11]. A precise method for this is the measurement of resonance frequencies of guided elastic waves in plates or plate-like structures. They sustain an infinite number of laterally propagating wave-modes, which are characterized by strongly non-linear dispersion curves $f = f(k)$. Here, f is the acoustic frequency and k the angular (in-plane) wavenumber. In elastically isotropic materials such guided waves are denoted as Lamb-waves [12, 13]. Resonances occur at frequencies associated with local minima of the dispersion curves, i. e., at points where their group velocity $v_g = 2\pi \partial f / \partial k$ vanishes. Depending on the elastic properties, in some dispersion branches, such minima can occur at points with a non-zero wavenumber (finite wavelength), and they are called zero-group velocity (ZGV) resonances [14, 15, 16, 17]. Excited with a local acoustic source, their wave-motion remains confined in the excitation region, and they can thus be considered as local [17]. As their frequency f_{ZGV} inversely scales with the local plate thickness h [13, 18], relative thickness changes can be locally probed by measuring the ZGV resonance frequency

*Corresponding author

✉ guqi.yan@recendt.at (G. Yan); clemens.gruensteidl@recendt.at (C. Grünsteidl); georg.watzl@recendt.at (G. Watzl); kevin.squoia@gat.com (K. Sequoia); pavel.lapa@gat.com (P. Lapa)

ORCID(s): 0000-0002-3632-2891 (M. Rzy); 0000-0002-5029-2609 (G. Yan)

f_{ZGV} and using the relation [16]

$$\frac{\Delta f_{\text{ZGV}}}{f_{\text{ZGV}}} = -\frac{\Delta h}{h}. \quad (1)$$

Laser ultrasonic (LUS) techniques [10, 19] are particularly well suited for that task, as they can provide local acoustic generation and detection [16]. Based on that technique, thickness measurements of mm- [20] or sub-mm thick metallic plates [21], imaging of μm -range thickness variations in a silicon wafer [22], or sub-micron layer on a substrate thickness variation measurements [23] have been demonstrated. Apart from that, a multitude of other laser ultrasonic, ZGV-based material characterization methods have been developed in the last two decades [24, 25, 26, 27, 28], including elastic constant characterization [29, 30, 31, 32].

Guided waves including ZGV-resonances have also been studied in curved plates like hollow cylinders, or spherically curved shells. If the relative thickness, which is the ratio of plate-thickness h and outer radius R , is low, guided waves approximately behave like in straight plates. Neglecting circumferential modes, they can be described by Lamb's theory. The larger the relative thickness, the stronger the deviation is, and the effect is more pronounced for low frequencies (large wavelengths) [33, 34, 29, 30]. For instance, Čes et al. showed that even for a hollow Zirconium alloy cylinder with a relative thickness of 12 %, the first ZGV-resonance frequency deviates less than 0.1 % from its straight-plate counterpart [30].

Most LUS techniques rely on pulsed laser excitation, with typical pulse durations ranging from the ns- to fs-scale. This results in broadband excitation of acoustic frequencies typically in the MHz to low GHz range, with some specialized system reaching into the low THz range [35, 36, 37]. However, generating acoustic signals with sufficient signal-to-noise ratio often requires sample ablation. But in cases where ablation damage is unacceptable, and only a narrow frequency band is required, e. g. when measuring single resonances, time-domain LUS may not be optimal. Frequency domain laser ultrasound (FréDomLUS) offers an alternative, which circumvents the mentioned issues by using a time-harmonic intensity modulated low power excitation laser in combination with phase sensitive detection. This way, narrow bands around an acoustic resonance can be probed directly in the frequency domain with a fine frequency resolution [38, 39, 40, 41, 26]. This technique was used to measure plate-resonances at GHz frequencies in fragile, micron-scaled plates for instance [40, 41, 26].

In this paper, we demonstrate ZGV-resonance based local wall thickness measurements in a spherical, hollow $80\ \mu\text{m}$ thin HDC-capsule with a frequency domain laser ultrasound (FréDomLUS) microscopy setup. In addition, broadband FréDomLUS measurements reveal the intriguing resonance landscape of the shell, that is analyzed with supporting finite element method (FEM) wave-propagation simulations, and numerical plate-dispersion calculations. We thereby identify local ZGV- and non-local circumferential resonances of the fundamental mode (SAW) and propose

Table 1

Elastic properties of high-density carbon [42] and calculated sound speeds.

Youngs's modulus	E	1050 GPa
Poisson's ratio	ν	0.10
density	ρ	$3515\ \text{kg/m}^3$
longitudinal speed of sound	c_L	$17\,479\ \text{m s}^{-1}$
transverse speed of sound	c_T	$11\,653\ \text{m s}^{-1}$
Rayleigh speed of sound	c_R	$10\,407\ \text{m s}^{-1}$

a simple method to isolate ZGV-resonances for local wall thickness determination. To the best of our knowledge, this is the first time that ZGV-resonance have been studied experimentally in a spherical shell.

2. Materials and methods

2.1. High-density carbon capsule sample

The investigated sample is a high-density carbon (HDC) spherical shell with a nominal diameter of 2 mm and a nominal wall thickness of $h = 80\ \mu\text{m}$ (see photograph and sketch in Fig. 1(a)). It contains a 0.38 at % W-doped internal layer with a thickness of about $6\ \mu\text{m}$. The HDC originates from Diamond Materials GmbH (Freiburg, Germany) and was further processed by General Atomics (San Diego, USA) to yield the shell-geometry [3]. The capsule diameter was measured with a micrometer screw gauge at ten random positions, yielding a diameter of $2R = (2.254 \pm 0.006)\text{mm}$, giving a relative thickness $h/R \approx 7\ %$. For laser-ultrasonic experiments, the capsule is placed on a mechanical rotation stage, which enables us to perform ultrasonic measurements along the circumference of the shell. For the sake of simplicity, we neglect the W-doped layer in any numerical calculations (sections 2.3 and 2.4), and use the elastic properties of pure HDC instead (see Tab. 1).

2.2. Frequency domain laser ultrasound experiments

For the measurement of local acoustic response spectra, we use a frequency domain laser ultrasound microscopy setup (Fig. 1b), which has been described in more detail elsewhere [38, 39, 41]. For thermoelastic excitation of ultrasonic waves, an electro-absorption intensity modulated laser diode with a wavelength of 1550 nm is amplified by an erbium-doped fiber amplifier (EDFA) to about 200 mW peak-to-peak power. It is focused by microscope objective to a spot with a diameter of approximately $2\ \mu\text{m}$ onto the HDC-capsule's surface. A time-harmonic modulation signal is provided by a vector network analyzer (VNA). The laser source thermo-elastically couples into elastic waves sustained in the sample at the same frequency f . The induced surface normal displacement is detected by a path-stabilized Michelson-Interferometer [43] which uses a 532 nm continuous-wave laser that is co-aligned with the excitation laser. The initial 120 mW detection laser is attenuated to 13.5 mW with neutral density filters, and

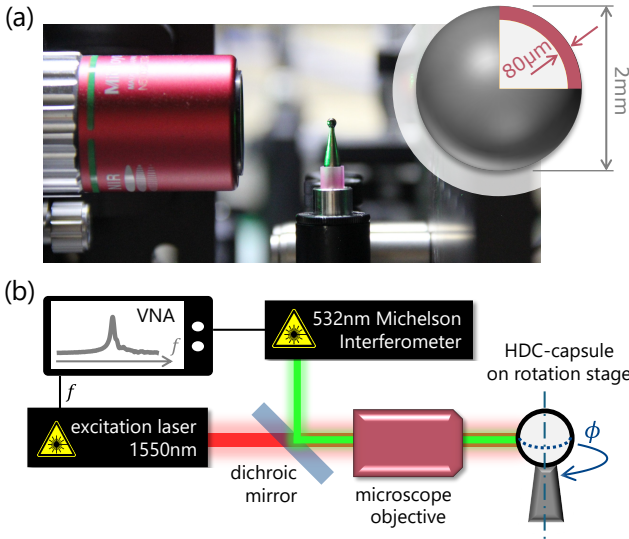


Figure 1: (a) Close-up of the HDC-capsule in front of the microscope objective and a sketch showing its geometry and dimensions (inset). (b) Sketch of the FreDomLUS-Setup used for thermoelastic excitation and detection of the ultrasonic frequency response of an HDC-capsule. The capsule is placed on a manual rotation stage for point-wise measurements along its circumference.

approximately half of the optical power impinges on the sample. The VNA records the Michelson's output in a phase-sensitive manner, yielding a complex voltage $\tilde{U}_{\text{VNA}}(f)$ which is proportional to the surface normal displacement $\tilde{u}_r(f)$, where the subindex r denotes the radial direction. To retrieve an acoustic response spectrum, the modulation frequency f is swepted.

2.3. Plate dispersion calculations

For the calculation of the elastic guided wave dispersion curves in straight HDC plates with the same thickness as the HDC-capsule, we use the MATLAB-toolbox *GEWtool* developed by Kiefer et al. [44]. It is based on a semi-analytical spectral elements method (SEM) and enables a fast calculation of dispersion curves, i.e., of all pairs of acoustic frequency f and in-plate-direction wavenumber k , which are sustained by the plate. In addition, the location of ZGV-points and the group velocity (v_g) can be computed [45, 46]. The isotropic elastic properties as stated in Tab. 1 have been used for all computations.

2.4. Finite element modeling

In addition to the SEM plate dispersion calculations, we simulate elastic wave propagation in spherical shells using finite element method (FEM) modeling. We assumed isotropic elastic behavior and used the mechanical properties specified in Tab. 1. Utilizing rotational symmetry along the y -axis, we reduced the problem to two dimensions (see Fig. 2). The outer sphere radius R was set to 1.127 mm in each simulation, and the shell thickness h was varied in different simulations. The spatial domain was discretized

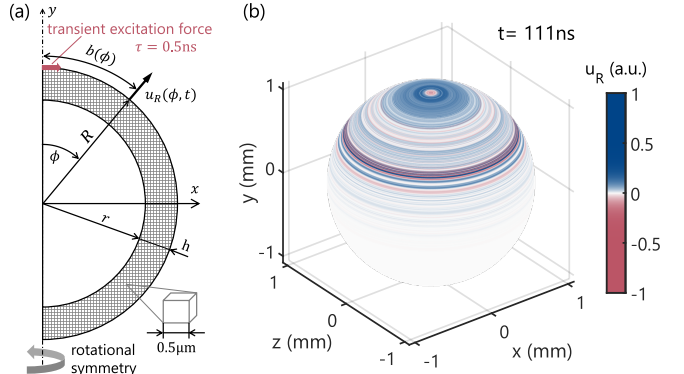


Figure 2: (a) Sketch of a finite element model of a HDC-capsule. (b) Snapshot of the radial displacement field on 80 μm thick HDC-capsule. An animation can be found online as supplementary in Sec. A.

into a structured mesh with 0.5 μm large cubic elements, resulting in models with around 10 million elements. This discretization corresponds to 83 elements per wavelength at the target maximal frequency of 250 MHz for the slowest wave, the Rayleigh surface acoustic wave. To emulate laser-based thermoelastic wave excitation, an in-plane (x -direction) force pulse with a spatiotemporal Gaussian profile with full width at half maximum of 2 μm and a duration of 0.5 ns (FWHM) was applied at the north pole ($x = 0, y = R$) of the shells. This approach is based on the work of Every et al. [47] and was successfully applied in previous FEM elastic wave propagation studies [48, 49]. The model was solved with the commercial FEM-solver PZFlex (Weidlinger Associates, Mountain View, CA) using an explicit central difference time-marching scheme. The time-step was set to 0.25 ns and the total simulation time to 10 μs, allowing the Rayleigh surface acoustic wave to orbit the sphere about 15 times. Computations were performed on a Intel Xeon W-2155 system (10 cores, 3.3 GHz) and typically took around 35 h per run. Figure 2(b) shows a snapshot of the radial displacement-field u_R in an 80 μm thick capsule 111 ns after wave excitation. The most pronounced ring corresponds to the surface acoustic wave.

2.5. Infrared interferometry reference measurements

As the HDC capsule is visually opaque, interferometric thickness measurements were conducted in the infrared spectral range, using wavelengths from 2 μm to 12 μm, where the material is sufficiently translucent. General Atomics previously custom modified a compact Fourier transform infrared (FTIR) spectroscopy system to allow high precision interference modulation measurements of the outer and inner wall-surface reflections. The instrument is capable of measuring HDC total wall thickness and sublayer thicknesses with a 5 nm precision [9, 50]. We use this modified FTIR system to characterize an HDC capsule wall thickness variation around a great circle surrounding the equator, as a reference for FreDomLUS measurements.

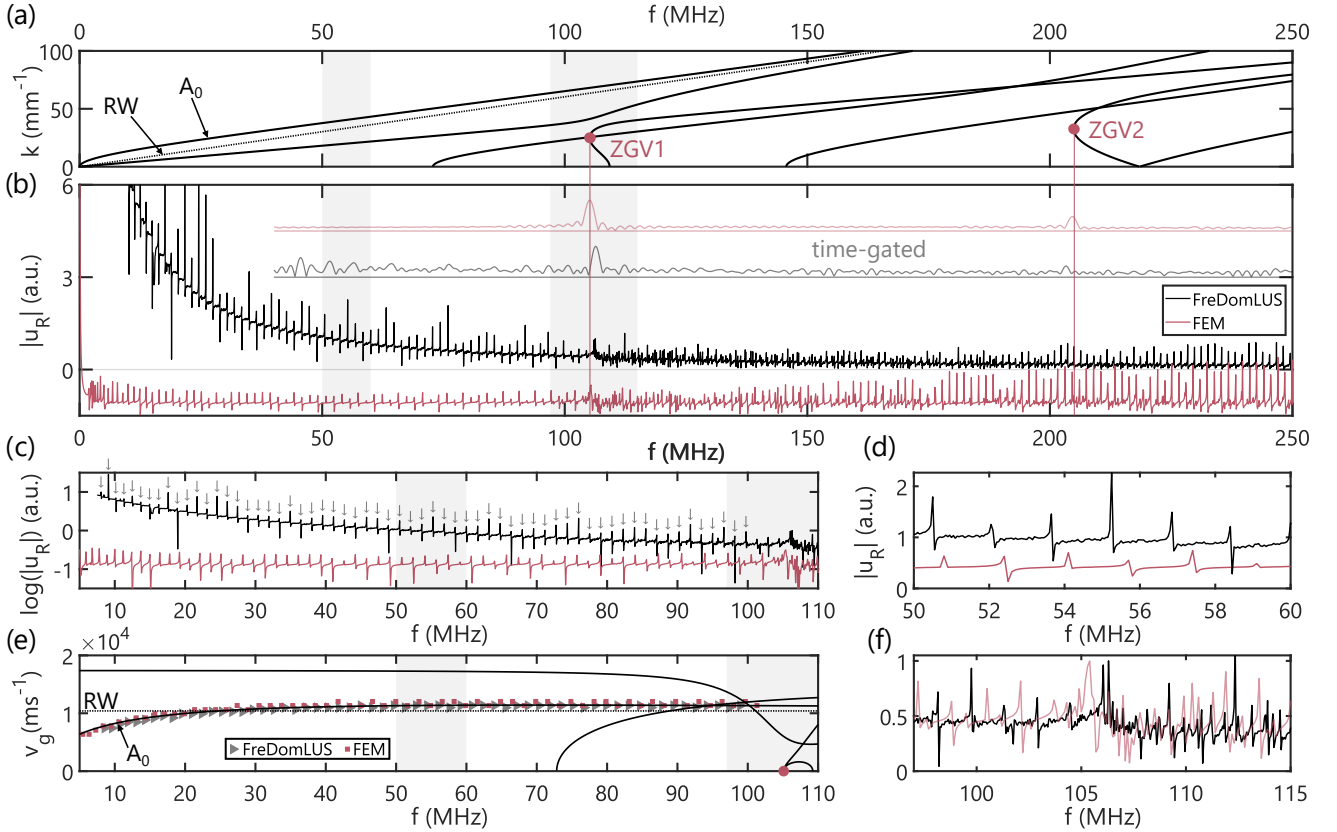


Figure 3: (a) Calculated elastic-wave dispersion (*GEWtool*) of a non-curved 80 μm thick HDC-plate. The fundamental mode (A_0) is marked with an arrow, and the first two ZGV-resonances (ZGV1 & ZGV2) with red dots. The dashed line corresponds to the Rayleigh surface acoustic wave (RW) of a semi-infinite half-space of the same material. (b,c,d,f) HDC-shell radial elastic response spectra up to a frequency of 250 MHz (FEM-trace is offset by a constant value), and time-gated versions of the same traces (shifted semi-transparent lines in the upper region of the graph). (c) Spectra up to 110 MHz showing multiple fundamental mode circumferential resonance peaks. Extracted resonance peak frequencies from the FreDomLUS spectrum are indicated by grey arrows. (d) Zoomed view of circumferential resonance peaks (frequency range is marked as grey area in (c)). (e) Calculated group velocity curves (*GEWtool*) of guided plate modes in a straight 80 μm thick HDC-plate. The grey (FreDomLUS) and black (FEM) data-points are group-velocities calculated from extracted circumferential resonance peaks. (f) Zoom to the frequency region around the ZGV1-resonance (marked as grey areas in (a,b,c,e)).

3. Results

3.1. Resonances on a spherical HDC shell

Figure 3(b) shows broadband single-point elastic response spectra recorded with a FreDomLUS microscopy setup (black solid line) and calculated from time-domain FEM simulations (red solid line) in a HDC-shell with the same dimensions ($R = 1.127$ mm, $h = 80 \mu\text{m}$). Both spectra are dominated by pronounced high quality factor peaks which cover the entire frequency range up to 250 MHz. Except for the slowly varying background in the experiment, which can be attributed to the thermoelastic generation, the spectra match well (the FEM-spectrum is offset by a negative constant value). The zoomed view in Figure 3(d) reveals a slight offset between the peaks in the measured and in the simulated spectrum. This slight mismatch can be expected, as the internal W-doped layer of the capsule was neglected in the FEM-model.

The low relative thickness of the shell ($\approx 7\%$) suggests that the curvature has only a minor influence on elastic wave propagation [34, 30]. It is thus useful to compare its frequency spectrum to the Lamb-wave dispersion of a straight plate to spot potential ZGV-resonance peak locations. This is shown in the top Fig. 3(a) for a 80 μm HDC-plate. The lowest order ZGV-resonances (denoted as ZGV1 and ZGV2) are marked by red dots in the figure. Apparently, the ZGV1-resonance at around 105 MHz aligns well with a spectral feature which clearly differs from the superimposed sharp peaks in its shape. However, this feature is not as pronounced and isolated as it is usually the case for ZGV-resonances in straight plates [16, 17, 21, 26, 20] (see magnified view in Fig. 3(f)).

It is thus instructive to study the nature of the spectral landscape in greater detail. We hypothesize, that like in solid spheres [51, 52], the multiple sharp peaks are caused by constructively interfering surface acoustic waves orbiting the

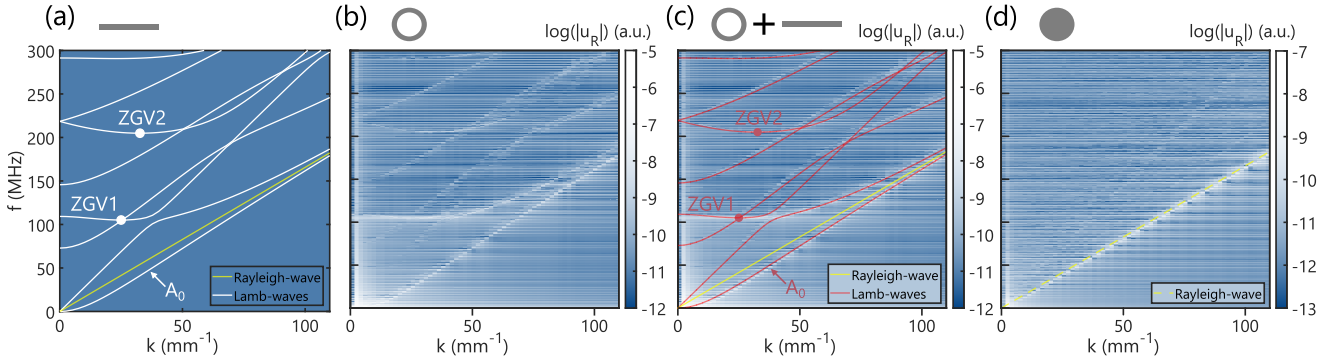


Figure 4: Elastic wave dispersion curves. (a) Calculated for a HDC-plate ($h=80\text{ }\mu\text{m}$) with the *GEWtool*. (b,c) For a HDC shell ($R=1.127\text{ mm}$, $h=80\text{ }\mu\text{m}$) obtained from a FEM simulation. In (c) the plate dispersion from (a) is superimposed as red family of lines. (d) Dispersion of a solid HDC sphere ($R=1.127\text{ mm}$) obtained from a FEM simulation. The y -axis are identical in each graph and have been omitted in (b-d) for space saving reasons.

spherical shell. The corresponding condition

$$n\lambda_n = 2R\pi \Leftrightarrow k_n = \frac{2\pi}{\lambda_n} = \frac{n}{R} \Leftrightarrow \Delta k = \frac{1}{R}$$

provides a rule for the determination of the group velocity from neighboring resonance peaks of the same mode, as

$$v_g = 2\pi \frac{\partial f}{\partial k} \approx 2\pi \frac{\Delta f}{\Delta k} = 2\pi R \Delta f. \quad (2)$$

We used this to extract the resonance peak locations with a maximum search algorithm for frequencies lower than the observed ZGV-feature (marked by small arrows for the FreDomLUS measurement in Fig. 3(c)) and used Eq. 2 for calculating the group velocity as a function of frequency. A comparison to the theoretical group velocity dispersion for a straight plate in Fig. 3(e) shows an excellent match between experimental- (grey triangles) and simulated-data (red squares) and the fundamental anti-symmetric plate mode (black solid line denoted as A_0) which converges to the Rayleigh-surface acoustic wave velocity for large frequencies (not shown the graph). The sharp peaks will thus be denoted as circumferential resonances from here on. Our observation agrees well with previous findings, where we have shown that the circumferential resonances can be effectively suppressed by embedding the capsule in a soft, damping material [53]. They further suggest that the curvature of the shell does not measurably influence wave-dispersion in the considered frequency range and thus may be neglected. Note that for frequencies beyond the ZGV1-point ($\gtrsim 105\text{ MHz}$) the circumferential resonance peaks get closer spaced in frequency. As this behavior starts at the ZGV1-frequency we attribute it to additional circumferential resonances established by propagating Lamb-modes from the ZGV1 dispersion branch.

A more comprehensive picture about the shell wave modes can be obtained from dispersion analysis. For that we transformed the radial displacement field obtained from the FEM-models, $u_R(b(\phi), t)$ from the physical domain to the reciprocal space to obtain $u_R(k, f)$ by two-fold fast Fourier transform (FFT). Here, the wavenumber k is the reciprocal

quantity of the arc length $b=b(\phi)$ (see Fig. 2(a)). As shown in Fig. 4(b), the resulting dispersion of the shell contains the strongly non-linear modes like those of a straight plate (Fig. 4(a)). In addition, a multitude of horizontal lines appear, which stem from the circumferential resonances. For better comparability, plate and shell-dispersion are superimposed in (Fig. 4(c)). Here, slight deviations between the Lamb-like modes in the shell and those of the straight plate are revealed. We attribute this to the curvature of the shell. But most importantly, the first two ZGV-points clearly exist in the shell's dispersion. Thus, we conclude that observed spectral feature in measurements and simulations around 105 MHz (see Fig. 3(b,f)) is caused by a ZGV-resonance. For sanity checking, we additionally conducted FEM simulations in a solid sphere with the same size as the capsule. As expected, its dispersion (Fig. 4(d)) contains horizontal circumferential modes, but not the non-linear plate modes. Here, the circumferential resonance are created by a non-dispersive SAW which appears as pronounced straight line in the dispersion and matches well with the Rayleigh-SAW of a semi-infinite solid. We conclude from the dispersion analysis, that the shell's dispersion landscape may be considered as a superposition of a solid sphere's dispersion and the dispersion of a straight plate, in that sense, that both, plate-resonances and circumferential resonances appear.

Having revealed the nature of the observed shell resonances, we can isolate the ZGV-resonance from the superimposed circumferential resonances by employing their different build-up times. While ZGV-resonances can be considered as constructively interfering bulk waves, being back and forth reflected from the quasi-parallel shell surfaces [54], the circumferential resonances originate from slower propagating guided waves (the fundamental mode A_0) which travel a larger distance around the circumference before interfering which one another. Hence, they require more time to build-up, and we can suppress them by selecting only early contributions in time-domain signals ('time-gating'). We therefore inverse fast Fourier transform (iFFT) acoustic spectra to the time domain, and back-transform only signals earlier than a certain gate-time. This has been done for the

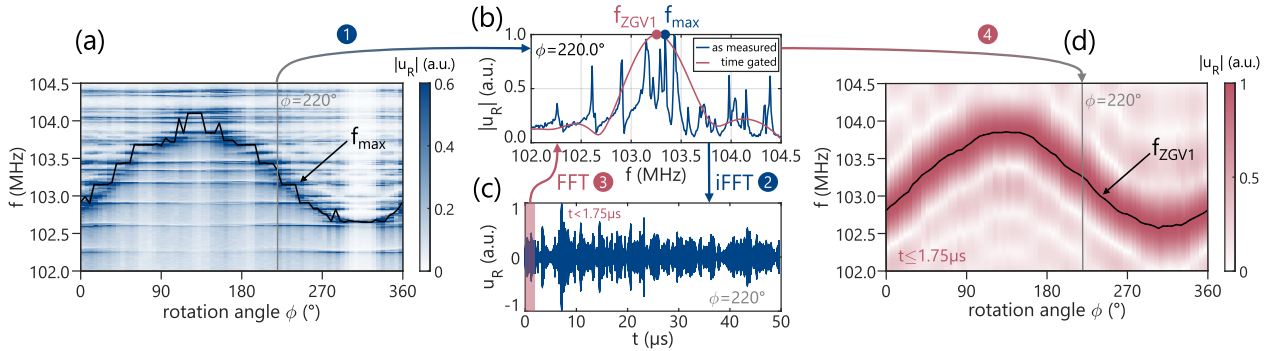


Figure 5: (a) Narrow-band FréDomLUS-measured acoustic response spectra in the range of the ZGV1-resonance, recorded along the HDC-shell equator. The spectra are normalized to their maximum magnitudes (black solid line). (b) Example spectrum recorded at a rotation angle of $\phi=220^\circ$. (c) Time-signal of the spectrum in (b), obtained by inverse fast Fourier transformation. The shaded red area indicates the fraction of the signal which is selected prior back-transformation. The time-gated spectrum is plotted as red solid line in (b). (d) Time-gated acoustic response spectra as function of rotation angle ϕ . The black solid line indicates the extracted ZGV1-resonance frequency. The sequence of the applied data-processing steps is indicated by the numbers ① – ④.

broadband spectra shown Fig. 3(b) by selecting time domain signal with $t < 0.55 \mu\text{s}$. In both resulting spectra (denoted as 'time-gated') the sharp circumferential resonance peaks have vanished, while the ZGV1-resonance remains. In addition, a second ZGV2-resonance has appeared, which was not visible in the unprocessed spectra. Note that while both ZGV-resonance peaks in the FEM spectrum perfectly match the plate dispersion predictions (Fig. 3(a)), the experimental resonances are slightly off. As the center-frequency ratio of two independent resonances in a homogeneous plate (like the observed the ZGV1 and ZGV2 resonances) is a unique function of Poisson's ratio [29, 32], we can estimate Poisson's ratio by using a numerically calculated calibration curve (see for example Fig. 4 in reference [29]). With $f_{\text{ZGV2}}/f_{\text{ZGV1}} \approx 1.91$ we obtain an effective Poisson's ratio of $\nu \approx 0.16$ instead of $\nu=0.1$ as given in Tab. 1. This deviation may be caused by altered mechanical properties caused by the slight W-doping of the HDC-capsule.

3.2. ZGV-resonance wall thickness measurements

For mapping the HDC-shell wall thickness, we recorded narrow-band acoustic spectra around the ZGV1-frequency with the FréDomLUS microscopy system along the equator of the HDC-shell. Therefore, the shell was rotated in $\Delta\phi = 5^\circ$ steps. The resulting spectra are shown in a 2D-map in Fig. 5(a). In addition to position independent circumferential resonance-peaks, which emerge as horizontal lines in the plot, the map clearly shows the varying ZGV1-resonance feature, linked to a wall thickness change. Figure 5(b) depicts an example spectrum, recorded at an rotation angle of 220° . Here, the ZGV-resonance is clearly superimposed by circumferential resonances, and by simply selecting the maximum peak frequency f_{max} (blue dot in Figure 5(b)), only a rough approximation the ZGV1-resonance frequency can be obtained. This is vividly illustrated in Figure 5(a), where the black f_{max} -line always snaps to the nearest circumferential resonance position. We thus point out that for getting precise

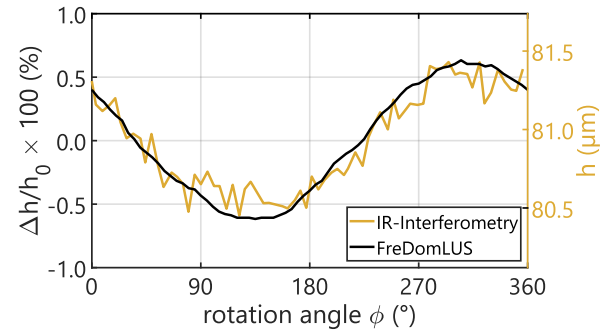


Figure 6: Measured relative (left y-axis) and absolute (right y-axis) wall thickness of a HDC-shell with an average diameter of 2.254 mm. Calculated from ZGV1-resonance center frequencies obtained from FréDomLUS-measurements (black solid line) and measured by IR-interferometry (yellow solid line).

wall thickness results, it is necessary to isolate the ZGV-resonance from the circumferential resonances by the time-gating procedure as described before. Here, we choose a cut-off time of $1.75 \mu\text{s}$ (Fig. 5(c)) which corresponds to around 2.8 round-trips of the SAW (A_0 -mode, with a maximum group velocity of $11\,414 \text{ m s}^{-1}$), and to 127 back and forth reflection of the transverse bulk wave. This suppresses the circumferential resonances in the processed spectrum, while the ZGV1-resonance remains (red line in Fig. 5(b)). Note that the ZGV1-peak is artificially broadened due to the use of a finite time-window. However, this does not alter the location of the ZGV1-peak maximum f_{ZGV1} . The latter is clearly shifted compared to the unprocessed spectrum. Finally, in the processed 2D-map (Fig. 5(d)) the circumferential resonances have vanished, while the varying ZGV1-peak remains, and the extracted ZGV1 center peak progression is substantially smoother than in the unprocessed map (compare black f_{max} and f_{ZGV1} curves in (a) and (d)).

As shown in Sec. 3.1, the guided modes in a curved shell behave like Lamb waves in the relevant frequency range.

Thus, we use the inverse plate-thickness scaling law (Eq. 1) to calculate the relative wall thickness change along the equator of the HDC-shell via (see Appendix B for further validation)

$$\frac{\Delta h}{h_0} = \frac{h(\phi) - h_0}{h_0} = -\frac{f_{\text{ZGV1}}(\phi) - f_{\text{ZGV1,0}}}{f_{\text{ZGV1,0}}}. \quad (3)$$

Here, we use the average ZGV1-frequency $\langle f_{\text{ZGV1}} \rangle_\phi = 103.22 \text{ MHz}$ as reference frequency $f_{\text{ZGV1,0}}$. The resulting black solid curve in Fig. 6 reveals a smooth wall thickness variation by a little more than 1 % along the capsule equator. To enable comparison to IR-interferometry reference wall thickness measurements, which provide an absolute measure (yellow line in Fig. 6, right hand side y-axis), we used its average result as a reference $h_0 = 80.93 \mu\text{m}$ to get $h(\phi)$ from Eq. 3. As shown in the plot, the results agree extraordinarily well and show a wall thickness variation of about $1 \mu\text{m}$ along the equator. Note that the FreDomLUS-measurement provides a smoother curve-progression than the reference measurement. To exclude, this is caused by an averaging effect due to the finite spatial resolution, which is governed by the lateral extent of the used resonance and not by the laser-spot sizes (provided that they are smaller), we calculate the latter. It can be estimated by half of the resonance wavelength [17, 55], given by $0.5\lambda_{\text{ZGV1}} = \pi k_{\text{ZGV1}}^{-1} = 125.7 \mu\text{m}$ (with $k_{\text{ZGV1}} = 25.0 \text{ mm}^{-1}$; see Fig. 3(a)). By using the measured capsule radius, this corresponds to an angular resolution of $\Delta\phi = 6.4^\circ$. As this is in the range of the measurement resolution (5.0° for FreDomLUS, and 5.1° for IR-interferometry), we assume that averaging effects can be neglected, and the FreDomLUS wall thickness measurement is more precise than the IR-reference method.

4. Discussion and Conclusion

We have presented an non-contact, local wall thickness variation measurement method for hollow spherical inertial confinement fusion targets based on a frequency domain laser ultrasound microscopy technique. It relies on the inverse scaling of the ZGV-resonance frequencies with the shell-thickness. For demonstration purposes, we scanned the first ZGV-resonance at around 106 MHz along the equator of a 2.154 mm-diameter W-doped HDC capsule with an average wall thickness of $81 \mu\text{m}$ (relative wall thickness of 0.7 % with respect to its radius). We found wall thickness variations of around 1 % and an excellent match to IR-interferometry reference measurements.

To justify our approach, relying on the applicability of Lamb's theory for infinite, non-curved plates, we carefully studied the inherently twofold-resonant nature of spherical shells. For that purpose we combined plate-wave dispersion calculations, FEM wave propagation simulations and experimental observations. We showed that in the considered frequency range from about 5 MHz to 250 MHz and for the specific normalized curvature (relative shell thickness) of $h/R \approx 7\%$, the shell's dispersion comprises of non-linear branches that closely match those of a straight plate.

In addition, it contains circumferential resonances which are a consequence of the closed-loop surface that sets an additional resonance condition for propagating Lamb-modes orbiting the shell. These resonances emerge as multiple high quality factor peaks in broadband acoustic spectra that obscure the required ZGV-resonances. We demonstrated that the different build up times of the two resonance species can be used to effectively isolate ZGV-resonances by selecting early contributions in time-domain signals.

A second ZGV-resonance at $\approx 203 \text{ MHz}$ was revealed after signal-processing and has been used to estimate the Poisson's ratio of $\nu = 0.16$, substantially deviating from the HDC literature value of 0.10. This indicates a modulation of the elastic parameters by the internal W-doped layer. In future work, we plan to assess the potential of using the circumferential resonances from single-point, broadband spectra for elastic characterization. For instance, by extracting the circumferential resonance peaks up to the first ZGV-resonance, which were shown to belong to the anti-symmetric fundamental mode (A_0) and can be used to calculate its group velocity. Simultaneously fitting the A_0 group velocity and the two observed ZGV-resonance frequencies with a fast plate-dispersion forward model may be used to determine the elastic constants and the average wall thickness of the shell, provided that the shell's outer sphere surface is perfect.

Since for sufficiently large frequencies the A_0 -mode can be considered as a surface acoustic wave propagating on the outer shell boundary, it must be affected by its geometry. Thus, we hypothesize that the A_0 -mode circumferential resonance quality factors may be used to detect deviations from a perfect spherical geometry.

The lateral resolution of the wall thickness measurement method can be estimated by half of the used S_1S_2 ZGV-resonances wavelength and was found to be around $126 \mu\text{m}$. This can be potentially improved by about 20 % by using the lower wavelength second ZGV-resonance.

Finally, we point out that the method can be applied to optically opaque materials like metals, or metal-doped HDC, where optical wall thickness characterization methods are limited due to low penetration depths.

CRediT authorship contribution statement

Martin Ryzy: Conceptualization (lead); Writing - original draft (lead); Writing – Review & Editing (equal); Project administration (lead); Supervision (equal); Funding acquisition (equal); Investigation (equal); Software (lead); Visualization (lead); Methodology (lead). **Guqi Yan:** Writing – Review & Editing (lead); Investigation (lead); Data curation (lead); Software (equal); Visualization (equal). **Clemens Grünsteidl:** Writing – Review & Editing (supporting); Validation (supporting). **Georg Watzl:** Writing – Review & Editing (supporting); Validation (supporting). **Kevin Sequoia:** Writing – Review & Editing (supporting); Resources (equal); Validation (supporting). **Pavel Lapa:** Writing –

Review & Editing (supporting); Resources (equal); Validation (supporting). **Haibo Huang:** Conceptualization (equal), Writing – Review & Editing (supporting); Project administration (equal), Supervision (lead); Funding acquisition (lead); Resources (equal), Validation (supporting).

Acknowledgements

This collaborative work is supported by General Atomics Internal R&D fund and is co-financed by the project “HyperMAT” by the federal government of Upper Austria and the European Regional Development Fund (EFRE) in the framework of the EU-program IBW/EFRE & JTF 2021-2027. The spherical HDC coating were produced by Diamond Materials GmbH, General Atomics laser drilled, leached the article into a capsule, built into Capsule-Fill-Tube-Assembly (CFTA), then into fully assembled targets for National Ignition Facility (NIF) shots under US Department of Energy (DOE) contract No. 89233124CNA000365. The authors would like to thank Marc Choquet (Tecnar) for initiating the collaboration between GA and RECENDT, and Robert Holzer (RECENDT) for taking a high-quality photo of our sample. For all figures, we used a high-contrast color-scheme which is suitable for people with impaired color vision as proposed by Paul Tol (<https://sronpersonalpages.nl/~pault>).

Declaration of competing interest

The authors declare that they have no competing financial interests or personal relationships that could have appeared to influence the work reported in this paper.

Data availability

Data will be made available by the authors upon reasonable request.

A. Supplementary data

A supplementary video to this article can be found online.

B. Validation ZGV-frequency scaling law

To confirm the validity of Eq. 1 we performed a series of FEM-simulations where we varied the shell-thickness h in 0.5 μm steps from 80 μm to 82 μm . From time-gated spectra (as shown in Fig. 3(b)) we extracted the ZGV1-frequency by maximum search. Figure 7 shows that the negative relative change of the ZGV1-resonance frequency ($-\Delta f/f$) linearly scales (with a slope of 0.99) with the relative change of shell-thickness ($\Delta h/h$). Thus, Eq. 1 approximately holds for the studied range of wall thickness variations.

References

1. Hurricane, O.A., Patel, P.K., Betti, R., Froula, D.H., Regan, S.P., Slutz, S.A., et al. Physics principles of inertial confinement

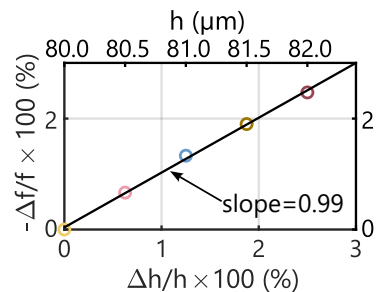


Figure 7: Validation of inverse scaling of the ZGV1-resonance frequency with shell-thickness with FEM simulations. The colored data-points correspond to ZGV1-resonance frequencies extracted from simulated broadband spectra of HDC-capsules with corresponding thickness h (see time-gated FEM-trace in Fig. 3(b) for instance).

fusion and U.S. program overview. *Reviews of Modern Physics* 2023; **95**(2):025005. doi:[10.1103/RevModPhys.95.025005](https://doi.org/10.1103/RevModPhys.95.025005).

2. Abu-Shwareb, H., Acree, R., Adams, P., Adams, J., Addis, B., Aden, R., et al. Achievement of Target Gain Larger than Unity in an Inertial Fusion Experiment. *Physical Review Letters* 2024; **132**(6):065102. doi:[10.1103/PhysRevLett.132.065102](https://doi.org/10.1103/PhysRevLett.132.065102).
3. Biener, J., Ho, D., Wild, C., Woerner, E., Biener, M., El-dasher, B., et al. Diamond spheres for inertial confinement fusion. *Nuclear Fusion* 2009; **49**(11):112001. doi:[10.1088/0029-5515/49/11/112001](https://doi.org/10.1088/0029-5515/49/11/112001).
4. Ross, J.S., Ho, D., Milovich, J., Döppner, T., McNaney, J., MacPhee, A.G., et al. High-density carbon capsule experiments on the national ignition facility. *Physical Review E* 2015; **91**(2):021101. doi:[10.1103/PhysRevE.91.021101](https://doi.org/10.1103/PhysRevE.91.021101).
5. Cardenas, T., Schmidt, D.W., Loomis, E.N., Randolph, R.B., Hamilton, C.E., Oertel, J., et al. Progress Toward Fabrication of Machined Metal Shells for the First Double-Shell Implosions at the National Ignition Facility. *Fusion Science and Technology* 2018; **73**(3):344–353. doi:[10.1080/15361055.2017.1406251](https://doi.org/10.1080/15361055.2017.1406251).
6. Braun, T., Kucheyev, S., Shin, S., Wang, Y., Ye, J., Teslich Jr, N., et al. Tungsten doped diamond shells for record neutron yield inertial confinement fusion experiments at the National Ignition Facility. *Nuclear Fusion* 2023; **63**(1):016022. doi:[10.1088/1741-4326/aca4e4](https://doi.org/10.1088/1741-4326/aca4e4).
7. Kritch, A.L., Schlossberg, D., Weber, C., Young, C., Dewald, E., Zylstra, A., et al. Design of first experiment to achieve fusion target gain > 1 . In: Phipps, C.R., Gruzdev, V.E., editors. *High-Power Laser Ablation VIII*. Santa Fe, United States: SPIE. ISBN 978-1-5106-7185-0; 2024, p. 1. doi:[10.1117/12.3017211](https://doi.org/10.1117/12.3017211).
8. Tollefson, J. How the world's biggest laser smashed a nuclear-fusion record. *online* 2024;.
9. Casey, D.T., MacGowan, B.J., Sater, J.D., Zylstra, A.B., Landen, O.L., Milovich, J., et al. Evidence of Three-Dimensional Asymmetries Seeded by High-Density Carbon-Ablator Nonuniformity in Experiments at the National Ignition Facility. *Physical Review Letters* 2021; **126**(2):025002. doi:[10.1103/PhysRevLett.126.025002](https://doi.org/10.1103/PhysRevLett.126.025002).
10. Scruby, C.B., Drain, L.E.. *Laser Ultrasonics Techniques and Applications*. Adam Hilger; 1990. ISBN 0-7503-0050-7.
11. Cheeke, J.D.N.. Nondestructive Evaluation of Materials - Thickness Gauging. In: *Fundamentals and Applications of Ultrasonic Waves*. CRC Press; 2012, p. 402–407.
12. Viktorov, I.A.. *Rayleigh and Lamb Waves*. Ultrasonic Technology. Springer Science + Business Media, LCC; 1 ed.; 1967. ISBN 978-1-4899-5683-5.
13. Graff, K.F.. 8.1 Continuous waves in a plate. In: *Wave Motion in Elastic Solids*. New York: Dover Publications Inc. ISBN 0-486-66745-6; 1991, p. 431–463.
14. Tolstoy, I., Usdin, E.. Wave Propagation in Elastic Plates: Low and High Mode Dispersion. *The Journal of the Acoustical Society of America* 1957; **29**(1):37–42. doi:[10.1121/1.1908675](https://doi.org/10.1121/1.1908675).

15. Gibson, A., Popovics, J.S.. Lamb Wave Basis for Impact-Echo Method Analysis. *Journal of Engineering Mechanics* 2005; **131**(4):438–443. doi:10.1061/(ASCE)0733-9399(2005)131:4(438).

16. Prada, C., Balogun, O., Murray, T.W.. Laser-based ultrasonic generation and detection of zero-group velocity Lamb waves in thin plates. *Applied Physics Letters* 2005; **87**(19):194109. doi:10.1063/1.2128063.

17. Prada, C., Clorennec, D., Royer, D.. Local vibration of an elastic plate and zero-group velocity Lamb modes. *The Journal of the Acoustical Society of America* 2008; **124**(1):203–212. doi:10.1121/1.2918543. arXiv: <https://doi.org/10.1121/1.2918543>.

18. Every, A.G.. Intersections of the Lamb mode dispersion curves of free isotropic plates. *The Journal of the Acoustical Society of America* 2016; **139**(4):1793–1798. doi:10.1121/1.4946771.

19. Spytek, J., Ambrozinski, L., Pelivanov, I.. Non-contact detection of ultrasound with light – Review of recent progress. *Photoacoustics* 2023; **29**:100440. doi:10.1016/j.pacs.2022.100440.

20. Watzl, G., Rzy, M., Österreicher, J.A., Arnoldt, A.R., Yan, G., Scherleitner, E., et al. Simultaneous laser ultrasonic measurement of sound velocities and thickness of plates using combined mode local acoustic spectroscopy. *Ultrasonics* 2025; **145**:107453. doi:10.1016/j.ultras.2024.107453.

21. Grünsteidl, C., Berer, T., Hettich, M., Veres, I.. Determination of thickness and bulk sound velocities of isotropic plates using zero-group-velocity Lamb waves. *Applied Physics Letters* 2018; **112**(25):251905. doi:10.1063/1.5034313. arXiv: <https://doi.org/10.1063/1.5034313>.

22. Balogun, O., Cole, G.D., Huber, R., Chinn, D., Murray, T.W., Spicer, J.B.. High-spatial-resolution sub-surface imaging using a laser-based acoustic microscopy technique. *IEEE Transactions on Ultrasonics, Ferroelectrics, and Frequency Control* 2011; **58**(1):226–233. doi:10.1109/TUFFC.2011.1789.

23. Cès, M., Clorennec, D., Royer, D., Prada, C.. Thin layer thickness measurements by zero group velocity Lamb mode resonances. *Review of Scientific Instruments* 2011; **82**(11):114902. doi:10.1063/1.3660182.

24. Prada, C., Clorennec, D., Royer, D.. Power law decay of zero group velocity Lamb modes. *Wave Motion* 2008; **45**(6):723–728. doi:10.1016/j.wavemoti.2007.11.005.

25. Yan, G., Raetz, S., Groby, J.P., Duclos, A., Geslain, A., Chigarev, N., et al. Estimation via Laser Ultrasonics of the Ultrasonic Attenuation in a Polycrystalline Aluminum Thin Plate Using Complex Wavenumber Recovery in the Vicinity of a Zero-Group-Velocity Lamb Mode. *Applied Sciences* 2021; **11**(15):6924. doi:10.3390/app11156924.

26. Rzy, M., Veres, I., Berer, T., Salfinger, M., Kreuzer, S., Yan, G., et al. Determining longitudinal and transverse elastic wave attenuation from zero-group-velocity Lamb waves in a pair of plates. *The Journal of the Acoustical Society of America* 2023; **153**(4):2090–2100. doi:10.1121/10.0017652.

27. Thelen, M., Bochud, N., Brinker, M., Prada, C., Huber, P.. Laser-excited elastic guided waves reveal the complex mechanics of nanoporous silicon. *Nature Communications* 2021; **12**(1):3597. doi:10.1038/s41467-021-23398-0.

28. Yan, G., Raetz, S., Chigarev, N., Blondeau, J., Gusev, V.E., Tournat, V.. Cumulative fatigue damage in thin aluminum films evaluated non-destructively with lasers via zero-group-velocity Lamb modes. *NDT & E International* 2020; **116**:102323. doi:10.1016/j.ndteint.2020.102323.

29. Clorennec, D., Prada, C., Royer, D.. Local and noncontact measurements of bulk acoustic wave velocities in thin isotropic plates and shells using zero group velocity Lamb modes. *Journal of Applied Physics* 2007; **101**(3):034908. doi:10.1063/1.2434824.

30. Cès, M., Royer, D., Prada, C.. Characterization of mechanical properties of a hollow cylinder with zero group velocity Lamb modes. *The Journal of the Acoustical Society of America* 2012; **132**(1):180–185. doi:10.1121/1.4726033.

31. Grünsteidl, C., Murray, T.W., Berer, T., Veres, I.A.. Inverse characterization of plates using zero group velocity Lamb modes. *Ultrasonics* 2016; **65**:1–4. doi:10.1016/j.ultras.2015.10.015.

32. Watzl, G., Kerschbaummayr, C., Schagerl, M., Mitter, T., Sonderegger, B., Grünsteidl, C.. In situ laser-ultrasonic monitoring of Poisson's ratio and bulk sound velocities of steel plates during thermal processes. *Acta Materialia* 2022; **235**:118097. doi:10.1016/j.actamat.2022.118097.

33. Lamb, H.. On the vibrations of a spherical shell. *Proceedings of the London Mathematical Society* 1882; **s1-14**(1):50–56. doi:10.1112/plms/s1-14.1.50.

34. Towfighi, S., Kundu, T.. Elastic wave propagation in anisotropic spherical curved plates. *International Journal of Solids and Structures* 2003; **40**(20):5495–5510. doi:10.1016/S0020-7683(03)00278-6.

35. Scruby, C.B., Drain, L.E.. 5 Ultrasonic Generation by Laser. In: *Laser Ultrasonics Techniques and Applications*. Adam Hilger. ISBN 0-7503-0050-7; 1990, p. 223–324.

36. Grahn, H., Maris, H., Tauc, J.. Picosecond ultrasonics. *IEEE Journal of Quantum Electronics* 1989; **25**(12):2562–2569. doi:10.1109/3.40643.

37. Matsuda, O., Larciprete, M.C., Li Voti, R., Wright, O.B.. Fundamentals of picosecond laser ultrasonics. *Ultrasonics* 2015; **56**:3–20. doi:10.1016/j.ultras.2014.06.005.

38. Murray, T.W., Balogun, O.. High-sensitivity laser-based acoustic microscopy using a modulated excitation source. *Applied Physics Letters* 2004; **85**(14):2974–2976. doi:10.1063/1.1802387.

39. Rzy, M., Grabec, T., Österreicher, J.A., Hettich, M., Veres, I.A.. Measurement of coherent surface acoustic wave attenuation in polycrystalline aluminum. *AIP Advances* 2018; **8**(12):125019. doi:10.1063/1.5074180.

40. Grünsteidl, C., Rzy, M., Hettich, M., Berer, T., Veres, I.. Evaluation of elastic wave attenuation in the GHz range using zero-group-velocity resonances. In: *Proceedings of the Forum Acusticum*. Lyon, France: e-Forum Acusticum 2020; 2020, p. 2557–2560. doi:10.48465/FA.2020.0582.

41. Grünsteidl, C., Veres, I., Berer, T., Kreuzer, S., Rothmund, R., Hettich, M., et al. Measurement of the attenuation of elastic waves at GHz frequencies using resonant thickness modes. *Applied Physics Letters* 2020; **117**(16):164102. doi:10.1063/5.0026367.

42. Diamond Materials GmbH, Feiburg, Germany. <https://www.diamond-materials.com/en/cvd-diamond/mechanical/>; 2025.

43. Scruby, C.B., Drain, L.E.. 3.2.1 The Michelson interferometer. In: *Laser Ultrasonics Techniques and Applications*. Adam Hilger. ISBN 0-7503-0050-7; 1990, p. 76.

44. Kiefer, D.. GEWtool [Computer software]. 2023. doi:10.5281/zenodo.10114243.

45. Kiefer, D.A., Plestenjak, B., Gravenkamp, H., Prada, C.. Computing zero-group-velocity points in anisotropic elastic waveguides: Globally and locally convergent methods. *The Journal of the Acoustical Society of America* 2023; **153**(2):1386–1398. doi:10.1121/10.0017252.

46. Kiefer, D.A., Watzl, G., Burgholzer, K., Rzy, M., Grünsteidl, C.. Electroelastic guided wave dispersion in piezoelectric plates: Spectral methods and laser-ultrasound experiments. *Journal of Applied Physics* 2025; **137**(11):114502. doi:10.1063/5.0250494.

47. Every, A.G., Utégulov, Z.N., Veres, I.A.. Laser thermoelastic generation in metals above the melt threshold. *Journal of Applied Physics* 2013; **114**(20):203508. doi:10.1063/1.4832483.

48. Rzy, M., Grabec, T., Sedlák, P., Veres, I.A.. Influence of grain morphology on ultrasonic wave attenuation in polycrystalline media with statistically equiaxed grains. *The Journal of the Acoustical Society of America* 2018; **143**(1):219–229. doi:10.1121/1.5020785. arXiv: <https://doi.org/10.1121/1.5020785>.

49. Grabec, T., Veres, I.A., Rzy, M.. Surface acoustic wave attenuation in polycrystals: Numerical modeling using a statistical digital twin of an actual sample. *Ultrasonics* 2022; **119**:106585. doi:10.1016/j.ultras.2021.106585.

50. Abu-Shwareb, H., Acree, R., Adams, P., Adams, J., Addis, B., Aden, R., et al. Lawson Criterion for Ignition Exceeded in an Inertial Fusion Experiment. *Physical Review Letters* 2022; **129**(7):075001.

doi:10.1103/PhysRevLett.129.075001.

51. Shui, Y., Royer, D., Dieulesaint, E., Sun, Z.. Resonance of surface waves on spheres. In: *IEEE 1988 Ultrasonics Symposium Proceedings*. Chicago, IL, USA: IEEE; 1988, p. 343–346. doi:10.1109/ULTSYM.1988.49396.
52. Royer, D., Clorennec, D.. Theoretical and Experimental Investigation of Rayleigh Waves on Spherical and Cylindrical Surfaces. In: *1st International Symposium on Laser Ultrasonics: Science, Technology and Applications*. Montreal, Canada; 2008, p. 8.
53. Yan, G., Huang, H., Lapa, P., Squoia, K., Grünsteidl, C., Ryzy, M.. Investigation of Zero-Group-Velocity Resonance in Inertial Confinement Fusion Target Capsules with Frequency-domain Laser Ultrasound Microscopy. In: *Journal of Physics: Conference Series*; vol. 2966. 2025, p. 012007. doi:10.1088/1742-6596/2966/1/012007.
54. Rose, J.L.. *Ultrasonic Waves in Solid Media*. Cambridge University Press; 2004. ISBN 0 521 54889 6.
55. Cès, M., Clorennec, D., Royer, D., Prada, C.. Edge resonance and zero group velocity Lamb modes in a free elastic plate. *The Journal of the Acoustical Society of America* 2011;130(2):689–694. doi:10.1121/1.3607417.